Heliyon 10 (2024) e26722

Contents lists available at ScienceDirect

Heliyon

journal homepage: www.cell.com/heliyon

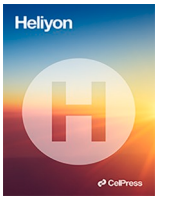

Research article

# On chip all-optical distinguishing of independently placed distinct types of single Rayleigh particle

Jannatul Shahrin Shoshi [a,1], M.R.C Mahdy [a,1,*], Mostafizur Rahman Rana [a]

[a] *Department of Electrical & Computer Engineering, North South University, Bashundhara, Dhaka, Bangladesh*

A B S T R A C T

In order to determine whether a particle is plasmonic, dielectric, or chiral, different complex processes and chemicals are applied in lab setups and pharmaceutical industries. Sorting or categorizing a particle based on distinct optical forces can be a novel technique. When a beam of light interacts with a particle, it usually pushes the particle in the direction of the light's propagation. Counterintuitively, it can also pull the particle toward the light beam or move it toward a lateral direction. As far as we know, to date, no comprehensive report exists regarding a single optical arrangement capable of inducing entirely distinct behaviors of force for three disparate types of independently placed single Rayleigh particle. This study introduces an all-optical technique aimed at effectively sorting nanoscale Rayleigh-sized objects employing a plasmonic substrate, when each distinct type of single particle is placed over the substrate independently. Unfortunately, this proposed technique does not work for the cluster or mixture of distinct particles. In our proposed configuration, a simple linearly polarized plane wave is incident onto the plasmonic substrate, thereby engendering completely different responses from three different types of nanoparticles: Gold (plasmonic), $SiO_2$ (dielectric), and Chiral particles. We conducted individual tests for our setup using linearly polarized plane waves at angles of 30-degree, 45-degree, and 60-degree individually. Consistent results were obtained across all angles. In each of the three distinct setups involving the aforementioned particle, a dielectric Rayleigh particle experiences an optical pulling force, a plasmonic Rayleigh particle experiences an optical pushing force, and a chiral Rayleigh particle encounters an optical lateral force. These distinctive force behaviors manifest as a result of the intricate interplay between the material properties of the nanoparticles and the characteristics of the plane-polarized beam, encompassing aspects such as plasmonic response, chirality, and refractive index. Moreover, this technique presents an environmentally sustainable and economically viable alternative to the utilization of expensive and potentially hazardous chemicals in nanoparticle sorting processes within industrial domains.

## 1. Introduction

In electromagnetism, optical manipulation refers to the use of electromagnetic radiation, such as light, to manipulate matter usually at the microscopic or nanoscopic scale. It relies on the interaction between light and matter, specifically the transfer of momentum from the photons of the light to the particles or molecules being manipulated. Optical micromanipulation is a technique that uses light to manipulate biomolecules [1–3], microscopic objects, and small particles [4]. It has become an important tool and grabbed the attention [5,6] in research areas such as biophysics and cell biology [7,8], nanotechnology [9], material science [10], microfluidics [11], chemistry [12,13] and quantum physics [14,15].

When light interacts with an object, it carries momentum and can exert a force on the object, resulting in a phenomenon known as radiation pressure [16]. Thus, the momentum of the photons in the light is transferred to the object, resulting in a change in the object's momentum and owing to momentum conservation [17–19]. The direction of radiation pressure is generally the same as the direction of the wave's propagation, meaning that the pressure acts in the same direction as the wave travels.

* Corresponding author.
*E-mail address:* mahdy.chowdhury@northsouth.edu (M.R.C Mahdy).
[1] These authors have contributed equally.

https://doi.org/10.1016/j.heliyon.2024.e26722
Received 10 October 2023; Received in revised form 18 February 2024; Accepted 19 February 2024
Available online 20 February 2024

But in the last decade, it has been observed that the direction of the movement of a nanoparticle can be quite different from the direction of wave propagation. A few Notable experiments [20,21] have been conducted to verify the counter-intuitive optical pulling force (also known as the tractor beam effect [17,22,23]), when a particle moves towards the opposite direction [24,25] of the propagation of light mainly due to the scattering force of light. In addition, optical lateral force has also been experimentally reported [24], when a particle experiences an optical force towards the perpendicular direction [26–29] of the propagating wave of light.

In real-world experimental setups and pharmaceutical industries (especially for chiral drugs), expensive compounds and chemicals are used extensively [30–33]. Usually, due to the tiny size of the particles and the requirement for high precision and accuracy, sorting methods [31] for particles, such as microplastics and gold nanoparticles, can be costly [34,35]. The idea of all-optical sorting instead of using expensive chemicals or compounds is quite new. Before the invention of the tractor beam effect and optical lateral force, such all-optical sorting was not even imagined to differentiate distinct types of particles based on distinct optical forces experienced by the particles.

Optical sorting [36] refers to the process of separating objects based on one or more characteristics, such as size, shape, or composition, by using light. There have been a few independent studies on the sorting of plasmonic [37], dielectric [38], and chiral particles (only dipolar-sized chiral particles) [26] separately based on optical force using various techniques and fully different optical setups. To the best of our knowledge, a single set-up to distinguish all of them together does not exist. For example-the half air-water set-up reported in Ref. [26] does not assist to distinguish dielectric or plasmonic Rayleigh or dipolar-sized particle. If a half-immersed dielectric or plasmonic particle is shined with light, it experiences an optical pushing force. This type of limitation is also true for the optical setups reported in Refs. [37,38].

In one of our previous studies, Rayleigh-sized particles were separated through near-field all-optical sorting from a cluster of three unknown particles [39]. Unfortunately, the dielectric particle from the cluster cannot be separated based on optical pulling force [39], if the plasmonic particle does not present in the heterogeneous cluster. Only the presence of the plasmonic particle in the cluster assists the near-field optical pulling of the dielectric particle according to the report of ref [39]. That means the all-optical sorting method used in Ref. [39] cannot distinguish a single Rayleigh particle based on its composition. After that, another study proposed a meta-surface that can sort only Mie-sized independently placed single particle based on their material properties and get force in three different directions (plasmonic-pulling, dielectric-pushing, and chiral-lateral) [40]. The set-up reported in Ref. [40], cannot sort Mie particles from the mixtures or clusters.

As far as we know, to date, no comprehensive report exists regarding a single optical arrangement capable of inducing entirely distinct behaviors of force for three disparate types of independently placed single Rayleigh particle. This presents a significant

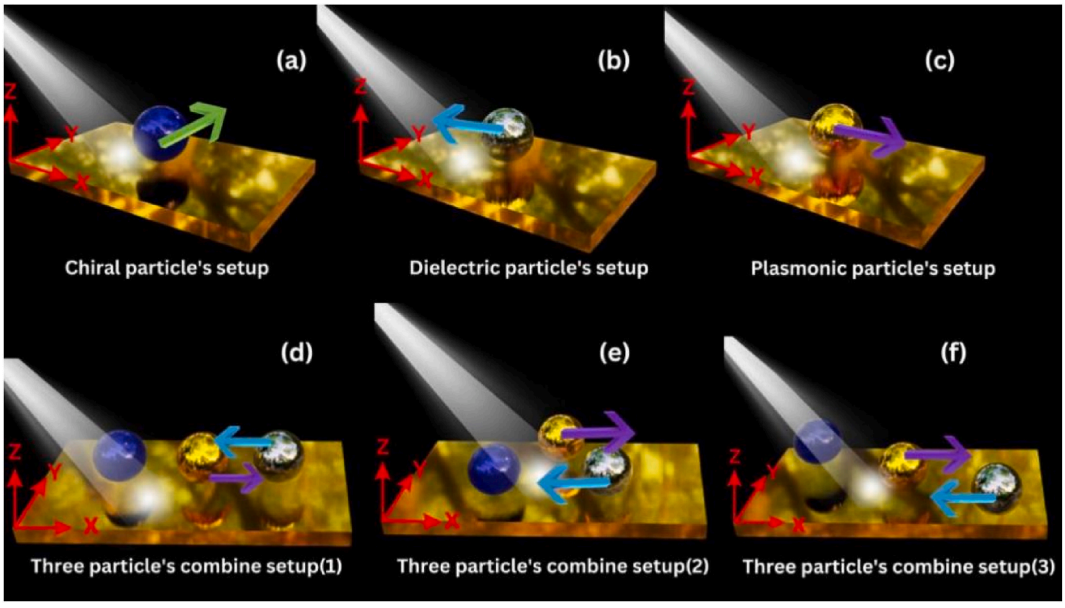


**Fig. 1.** Optical manipulation of particles on gold substrates using a plane-polarized (oblique incidence) laser beam of wavelength 632 nm propagating in the "+x" direction (a) A chiral particle on a gold substrate experiences an optical pulling force, which allows for precise control of particle motion and positioning. (b) A dielectric particle on a gold substrate experiences an optical pushing force. (c) A plasmonic particle on a gold substrate experiences lateral force due to the asymmetric interaction between the particle and the chiral plasmonic substrate, demonstrating the potential of plasmonic substrates for manipulating particles with complex geometries. (d) The setup consists of three particles (chiral, plasmonic, and dielectric) positioned in a serial arrangement on a gold substrate. (e) On a gold substrate, the same three particles are arranged in an angular pattern. (f) This figure shows the same particles positioned diagonally on the gold substrate. For all three particle setups, each particle experiences a different optical force: the dielectric particle experiences an optical pulling force, the plasmonic particle experiences an optical pushing force, whereas the chiral particle doesn't get any effective force. (For interpretation of the references to colour in this figure legend, the reader is referred to the Web version of this article.)

limitation in the field, as the ability to sort particles at this level would enable a range of new possibilities in fields such as biomedicine and materials science. Our study of this work seeks to address this gap in the literature.

In this work, the sorting of distinct types of Rayleigh-sized particles has been achieved through the use of three distinct types of optical forces: pulling, pushing, and lateral. Interestingly, this sorting does not require complex structured beams [22,41] or any kind of artificial meta-surface [40], as a simple time-harmonic plane linearly polarized laser beam along with a plasmonic substrate is sufficient for this system. It should be noted that the proposed setup involves the sorting of separately placed Rayleigh-sized objects, rather than a cluster [39] of different types of particles (recently reported by us). Different Rayleigh-sized particles in our proposed arrangement experience radically different optical forces over (near) a plasmonic substrate. The plasmonic particle experiences a pushing force due to the absence of current density reversal within a certain length; the dielectric particle experiences a pulling force due to the momentum contribution from the field-induced multipole radiation; and the chiral particle experiences a lateral force due to the electric field density and direction of the Poynting vector.

It is important to note that our proposed technique in this article does not work for the heterogenous cluster or mixture of distinct particles. This is because the chiral particle in a heterogeneous cluster of particles in our set-up does not experience enough lateral force due to the unwanted coupling and multiple scattering in the presence of other types of particles. A very interesting observation regarding this matter (the suppression of scattering) has been discussed in our article. For the heterogeneous cluster set-up, still the known approach of near-field all-optical sorting is the one reported [39], one of recent works. For homogeneous clusters of the same type of particles, the proposed setup of this work works very well (and our previously reported process of [39] does not work). But it (the work of this article) cannot be regarded as an efficient sorting or distinguishing process of distinct particles in an arbitrary cluster of unknown Rayleigh or dipolar particles. As a result, safely we can consider this work as an approach to single Rayleigh or dipolar particle sorting instead of the sorting of particles from a fully unknown cluster or mixture of Rayleigh or dipolar particles.

Optical sorting of Rayleigh or dipolar-sized particles could revolutionize future industrial techniques for sorting microplastics, gold nanoparticles, chiral molecules, and other similar particles. The unique optical forces experienced by each type of particle, as demonstrated in our study, could enable more efficient and precise sorting compared to existing techniques. Overall, the proposed plasmonic setup has the potential to impact various industries that require precise particle sorting, ranging from pharmaceuticals to environmental sustainability.

## 2. Optical setup and methods

In this article, we have demonstrated a unique optical setup and investigated the effect of different types of force on Rayleigh-ranged (i.e., dielectric, plasmonic, and chiral) nanoparticles placed on a plasmonic substrate. Three separate optical setups were used for each particle type, which involved placing the particles individually on three separate plasmonic substrates in Fig. 1(a–c). The length, width, and thickness of the plasmonic substrate are 200 nm, 150 nm, and 25 nm, while the radius of all the particles employed in our optical setup (plasmonic, dielectric, and chiral) is 25 nm (r = 25 nm). Furthermore, particles are individually positioned 5 nm vertically (surface-to-surface distance) from the plasmonic substrate. In Fig. 1(d–f), three more optical setups have been shown as another experiment to create distinct forces for the same three particles altogether.

These arrangements were designed to see if the particles experienced the same force on the same substrate as the single-particle setup. The dimensions of the plasmonic substrates (for three particles) are 450 nm, 300 nm, and 25 nm. The particles were positioned 5 nm above the substrate and had the same radius as a single particle configuration. On the plasmonic substrate, the particles are placed serially, angularly, and diagonally with an interparticle distance. For the cluster setup (serial-interparticle distance of 100 nm), the plasmonic nanoparticle is placed at the center of the substrate, the chiral nanoparticle is placed on the left side of the plasmonic nanoparticle, and the dielectric nanoparticle is placed on the right side of it. The source of illumination for our proposed optical setup is a non-structured time-harmonic plane linearly polarized laser beam with a wavelength of 632 nm, which propagates at distinct angles (i.e., 30-degree, 45-degree, 60-degree etc.) from the ''-x'' to the ''+x'' direction, has electric field polarization along the ''y'' direction, decays in the '-z' direction at the 'xz' plane, and can be expressed as:

$$\mathbf{E} = \mathrm{E}_0\left[\mathrm{e}^{-\mathrm{jk}(\mathrm{xcos\theta}-\mathrm{zsin\theta})}\right]\hat{\mathbf{y}} \tag{1}$$

Light intensity has been defined as $\mathrm{E}_0 = 1\ \mathrm{V/m}$. By utilizing the numerical solver COMSOL Multiphysics 5.3a, we have carried out full-wave simulations by varying the wavelength ($\lambda$) of the incident beam from 200 nm to 700 nm and evaluating the resulting optical force on the three distinct nanoparticles. In full-wave simulations, the optical forces calculated outside the volume of the aforementioned nanoparticles are referred to as time-averaged optical forces. The time-averaged optical force has been calculated by integrating the Minkowski stress tensor at an equal radius to the particle's radius plus 3 nm ($r = a^{+}$) [17,42–46].

$$\langle \mathrm{F}^{\mathrm{out}}_{\mathrm{Total}} \rangle = \oint [\langle \bar{\bar{\mathbf{T}}}^{\mathrm{out}} \rangle] \bullet \mathrm{ds} \tag{2}$$

Where $\langle \bar{\bar{\mathbf{T}}}^{\mathrm{out}} \rangle$ is expressed as:

$$\langle \bar{\bar{\mathbf{T}}}^{\mathrm{out}} \rangle = \frac{1}{2}\mathrm{Re}\left[\mathbf{D}_{\mathrm{out}}\mathbf{E}^{*}_{\mathrm{out}} + \mathbf{B}_{\mathrm{out}}\mathbf{H}^{*}_{\mathrm{out}} - \frac{1}{2}\bar{\bar{\mathbf{I}}}\left(\mathbf{E}^{*}_{\mathrm{out}} \bullet \mathbf{D}_{\mathrm{out}} + \mathbf{H}^{*}_{\mathrm{out}} \bullet \mathbf{B}_{\mathrm{out}}\right)\right] \tag{3}$$

The "out" can be defined as the total exterior field of the scatterer. $\bar{\bar{\mathbf{I}}}$ is the unity tensor, while '< >' indicates the time average. **E, D, B,**

and **H** refer to the electric fields, displacement vector, induction field vector, and magnetic field. The material properties of the dielectric nanoparticle have been defined as having a refractive index of n = 1.45. The chiral object has been specified as a right-handed chiral nanoparticle with a parameter value of 'k = 1'. The refractive index values for the plasmonic (Au) material and substrate have been obtained from the well-known Palik's data [47], encompassing both the real and imaginary components.

## 3. Result and discussion

A schematic view of three different particles (plasmonic as Au, dielectric as $SiO_2$, and chiral) positioned on a gold substrate is shown in Fig. 2, where 2(a) shows a serial arrangement of dielectric, plasmonic, and chiral particles in the (x-y) plane of the substrate, 2(c) shows the same particles positioned at an angular distance from each other, and 2(e) shows the same particles positioned in diagonally on the substrate. The wavelength ($\lambda$) of the incident beams has been varied from 200 nm to 700 nm, and the optical force exerted on the three nanoparticles has been calculated using COMSOL Multiphysics 5.3a.

By analyzing the results shown in Fig. 2(b–d, f), we can see that from 300 nm to 550 nm, the dielectric particle exhibits optical pulling force (in the -x direction), while the plasmonic particle exhibits optical pushing force (in the +x direction) for the same range. Consequently, we observe that dielectric (silica) and plasmonic (gold) nanoparticles on the plasmonic substrate exhibit both get pulling and pushing forces in various wavelength ranges. However, the chiral particle hardly ever experiences a force that is close to zero and can be neglected.

In contrast, an exceptional result was obtained for the chiral case on the plasmonic substrate. For three single particle setups shown in Fig. 3(a–c, e) depicts that at the range of 250 nm–500 nm, a single chiral particle experiences an optical lateral force, while the

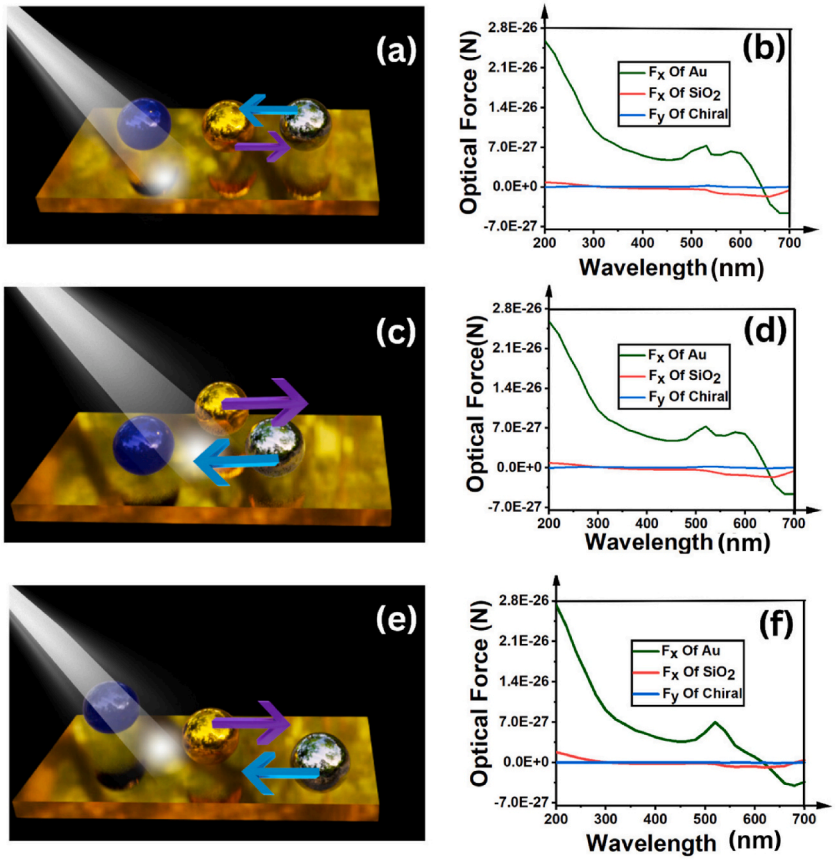


**Fig. 2.** Schematic view of three different particles (plasmonic as gold, dielectric as $SiO_2$, and chiral) set on a gold substrate and their corresponding optical force graphs when illuminated with a 45-degree plane polarized optical beam at a certain wavelength along the "+x" direction. (a) Shows a serial arrangement of dielectric, plasmonic, and chiral particles in the (x–z) plane of the substrate. (b) Depicts the graph of the configuration where the plasmonic particle experiences both pushing and pulling forces at various wavelengths, the dielectric experiences pulling from 300 nm to the end, and the chiral particle experiences negligible optical force (close to zero). The identical particles are displayed in (c) at an angular separation from one another, and the corresponding force graph is presented in (d), both of which illustrate the same outcome as the first. Again, the identical particles are displayed in this picture (e) arranged in a diagonal pattern on the substrate. The corresponding force graph is given in this figure (f), and the outcome is the same as previously. (For interpretation of the references to colour in this figure legend, the reader is referred to the Web version of this article.)

dielectric particle experiences an optical pulling force and the plasmonic particle experiences an optical pushing force in Fig. 3(b–d, f).

In both scenarios, the plasmonic particle experiences optical pushing forces in the '+x' direction. Beyond a certain wavelength, it encounters optical pulling forces in the '-x' direction. Additionally, in both cases, dielectric particles experience optical pulling forces ranging from 300 nm to 550 nm (for the three-particle setup) and from 250 nm to 550 nm (for the single-particle setup). However, for the single particle setup depicted in Fig. 3(a), an outstanding outcome was obtained for the chiral case on the plasmonic substrate which made the case successful. An additional lateral force is experienced by the chiral particle in the direction of "+y", as shown in Fig. 3(b). It means that when a single chiral particle is placed on a gold substrate alone, the incident laser beam on the gold substrate can affect the chiral particle. However, the force magnitude is insufficient to overcome Brownian motion or gravity. To address this limitation, we conducted numerical simulations in which we increased the amplitude of the plane waves, resulting in a higher force (Supplementary Note 1).

Table 1 represents the results of our simulations for both three-particle setups and single-particle setups, primarily focusing on the results generated by simulating the setups shown in Figs. 2 and 3. The table describes that the single-particle setups exhibit three distinct types of force for three distinct types of nanoparticles: lateral force for chiral, pulling force for dielectric, and pushing force for plasmonic. However, the three-particle setups did not produce any lateral force for chiral nanoparticles.

Furthermore, it is essential to recognize that maintaining a static configuration (only 45 degree of incident light) may not be a practically suitable example. Consequently, we have undertaken simulations with variable parameters, including a radius (r) of 50 nm and incident light angles (θ) of both 30° and 60° as illustrated in Fig. 4(a–i), to achieve a more realistic representation. In all instances, we have adhered to the same configuration as the one initially proposed in our primary simulation. It's important to note that throughout these variations, the plasmonic particle encounters an optical pushing force, the dielectric particle experiences an optical pulling force, and the chiral particle undergoes an optical lateral force. Additionally, we conducted a parametric evaluation of the

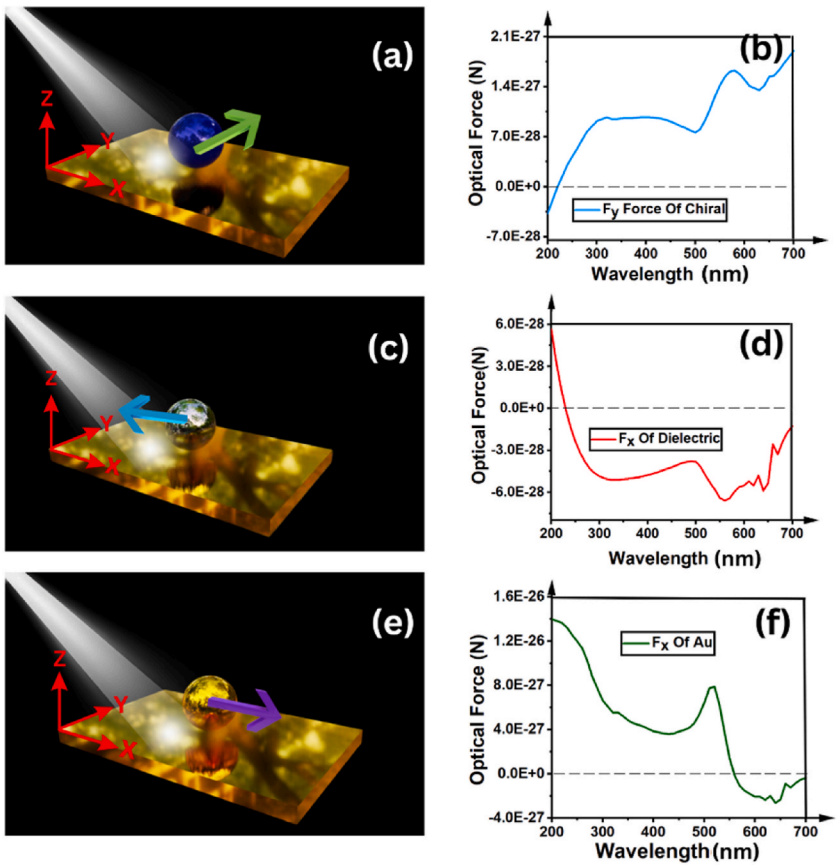


**Fig. 3.** Illuminating at a 45-degree angle with a plane-polarized light, (a) represents a schematic view of single chiral particles placed over a gold substrate, and (b) shows the outcome of the full-wave simulation for our proposed optical configuration, where chiral particle experiences optical lateral force toward the "+y" direction. The schematic image of a single dielectric particle placed on a gold substrate is shown in (c), and the outcome of the full-wave simulation for the optical configuration for our proposed set up is shown in (d), where the dielectric particle experiences an optical pulling force in the "-x" direction and (e) depicts a schematic image of a single plasmonic particle placed over a gold substrate. and (f) shows the outcome of the full-wave simulation for our proposed optical configuration, where plasmonic particle experience optical pushing force toward the "x" direction. The sorting domain for our optical setup is observed from 250 nm to 550 nm. (For interpretation of the references to colour in this figure legend, the reader is referred to the Web version of this article.)

**Table 1**
Optical comparison of the sorting range between three nanoparticles and a single nanoparticle placed over our proposed optical setup.

| Number of Particles | Particle Size | Chiral | Dielectric | Plasmonic | Substrate |
|---|---|---|---|---|---|
| Three particles | Rayleigh | Mainly pushing force | Pulling | Pushing | Plasmonic Substrate |
| Single particle | Rayleigh | Lateral | Pulling | Pushing | Plasmonic Substrate |

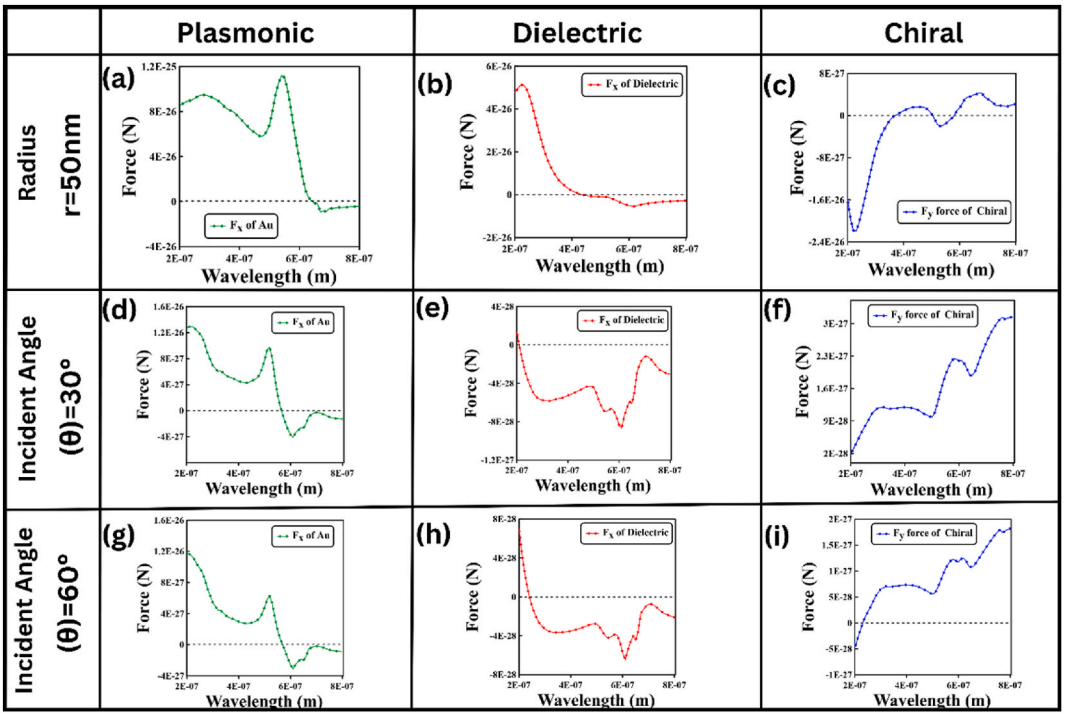


**Fig. 4.** Represents the results of full-wave simulations performed on our proposed optical configuration. In this setup, we varied the particle radius (r = 50 nm) with an incident angle of θ = 45°. We applied incident light angles of θ = 30° and θ = 60° to plasmonic, dielectric, and chiral particles, each with a 25 nm radius, arranged individually on a gold substrate. Panels (a–c) display the simulation outcomes for particles with a 50 nm radius at a θ = 45° incident light angle, while panels (d–i) demonstrate the results for all three particle types under incident light angles of θ = 30° and θ = 60° with a 25 nm radius. (For interpretation of the references to colour in this figure legend, the reader is referred to the Web version of this article.)

optical force behavior by varying the separation between our nanoparticles and the gold substrate (see Supplementary Note 2).

### *3.1. Sorting of single chiral particle: origin of the optical lateral force*

Drug discovery and development (for several industrial situations, which depend on the identification and isolation of specific chiral molecules) may be aided by the capacity to sort particles precisely and effectively. By ensuring that the desired components are present in the appropriate quantities, chiral sorting could aid in pharmaceutical product quality control.

A setup with a right-handed chiral particle is shown in Fig. 3(a). Our full-wave simulation results indicate that we have observed chiral lateral force (by applying the stress tensor method given in Eq. (2) in the scenario of a single particle chiral setup, as shown in Fig. 3(b)). The constitutive relation of a chiral particle can be described as [48,49]:

$$\mathbf{D} = \varepsilon_0 \varepsilon \mathbf{E} + ik\sqrt{\varepsilon_0 \mu_0}\mathbf{H}$$

$$\mathbf{B} = \mu_0 \mu \mathbf{H} - ik\sqrt{\varepsilon_0 \mu_0}\mathbf{E}$$

Here, ε and μ are the relative permittivity and permeability of the chiral material, respectively [$\mu = 1$ and $\varepsilon = (1.45)^2$]; The sign kappa "κ" is positive, negative, and nonzero when the chiral is right-handed, left-handed, or nonchiral and finally, $\varepsilon_0$ and $\mu_0$ are the permittivity and permeability in a vacuum.

The chirality parameter of the chiral particle, $\kappa = 1$, defines its chirality. It indicates the asymmetry of the particle's structure concerning its mirror image. Here, a light with a 45-degree oblique angle illuminates a chiral particle, which experienced a chiral lateral force at a wavelength of 250 nm. The interaction between the incident light and the chiral characteristic of the particle causes this force, which is perpendicular to the direction of light propagation. In this instance, energy moves from the incidence plane (x-z) to

the lateral plane (y-z). We also simulated the Poynting vector and figured out some interesting connections with the lateral force.

Our findings indicate that we only observed chiral lateral force in the scenario of a single particle chiral setup, as shown in Fig. 3(b). However, such lateral force on a chiral particle vanishes in the presence of the other particles near (over) the substrate. The physical reasoning behind the mentioned observations has been explained next step by step:

For a single dipolar chiral particle [cf. Fig. 4 for single particle case], the time-averaged total force considering the validity of dipole approximation:

$$\langle \mathbf{F}\ \text{Dipole (Generic)}\rangle = \frac{1}{2}\left[\text{Re}\left[(\nabla \mathbf{E}^*)\bullet \mathbf{p}\right] + \frac{1}{2}\text{Re}\left[(\nabla \mathbf{B}^*)\bullet \mathbf{m}\right] - \frac{k^4}{12\pi\varepsilon_0 c}\text{Re}\left[\mathbf{p}\times \mathbf{m}^*\right]\right] \tag{4}$$

where,

$$\begin{bmatrix}\mathbf{p}\\ \mathbf{m}\end{bmatrix} = \begin{bmatrix}\alpha_{ee} & i\alpha_{em}\\ -i\alpha_{em} & \alpha_{mm}\end{bmatrix}\begin{bmatrix}\mathbf{E}\\ \mathbf{H}\end{bmatrix}$$

$$\langle \mathbf{F}\rangle = \nabla U + \frac{\sigma\langle \mathbf{S}\rangle}{C} - \text{Im}[\alpha_{em}]\nabla\times\langle \mathbf{S}\rangle + c\sigma_e\nabla\times\langle \mathbf{L}_e\rangle + c\sigma_m\nabla\times\langle \mathbf{L}_m\rangle + \omega\gamma_e\langle \mathbf{L}_e\rangle + \omega\gamma_m\langle \mathbf{L}_m\rangle + \frac{ck_0^4}{12\pi}\,\text{Im}\left[\alpha_{ee}\alpha_{mm}^*\right]\text{Im}[\mathbf{E}\times\mathbf{H}^*]$$

Here, $U = 1/4(\text{Re}[\alpha_{ee}]|\mathbf{E}|^2 + \text{Re}[\alpha_{mm}]|\mathbf{H}|^2 - 2\text{Re}[\alpha_{em}]\text{Im}[\mathbf{H}.\mathbf{E}^*])$ is the term due to particle-field interaction, $\langle \mathbf{S}\rangle$ denotes the time-average Poynting vector, $\langle \mathbf{L}_e\rangle = \varepsilon_0/(4\omega i)(\mathbf{E}\times\mathbf{E}^*)$ and $\langle \mathbf{L}_m\rangle = \mu_0/(4\omega i)(\mathbf{H}\times\mathbf{H}^*)$ are the time-averaged spin densities

To comprehend the components of the optical lateral force acting on a chiral particle, a detailed analysis has been done; which suggests the spin angular momentum (SAM) and the Poynting vector as the responsible components for the lateral force [30]:

$$\mathbf{F}_{\text{lateral}} = \mathbf{F}_{\text{poynting}} + \mathbf{F}_{\text{SAM}} \tag{5}$$

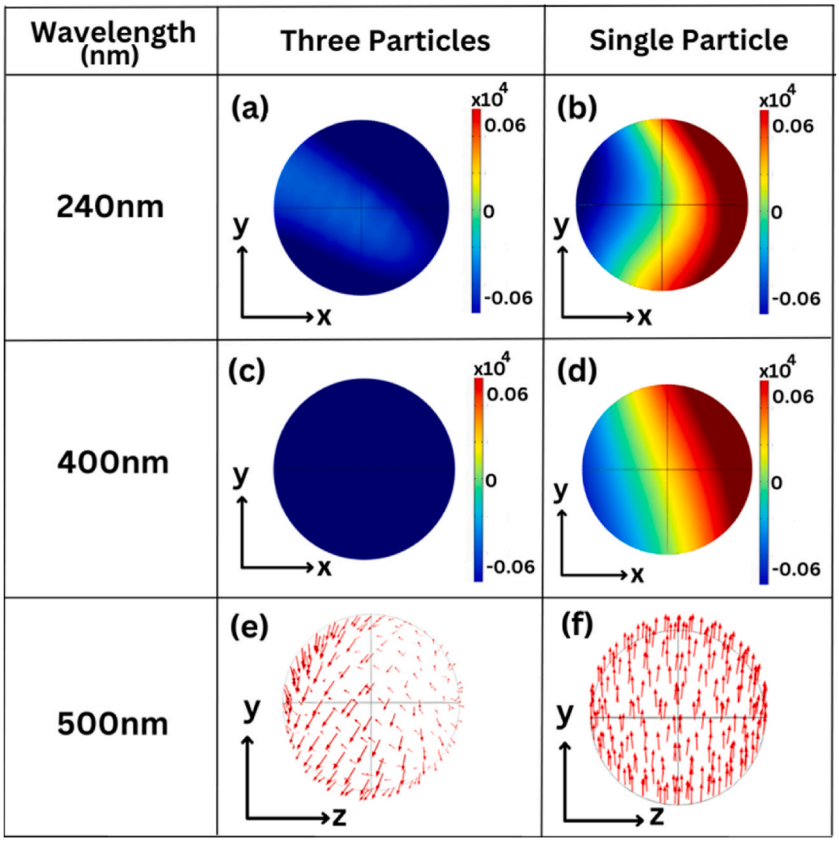


**Fig. 5.** Illustrates a full-wave simulation of the optical force on a chiral particle in both a three-particle arrangement and a single particle setup on a plasmonic substrate (note: the incident angle of light is set at 45°). (a) and (c), reveal that the electric field profile ($\mathbf{E}_x$) component has no impact on the chiral particle at 240 nm and 400 nm for the three-particle setup. (b) and (d) show that the electric field profile ($\mathbf{E}_x$) component creates a dipole on the chiral particle in the case of the single particle configuration at a wavelength of 240 nm and 400 nm. (e) It displays at 500 nm the three-particle setup's pointing vector arrows, each of which points in a distinct direction. That implies that there is no lateral force acting on the particle. (f) It indicates that the force is in the "y-z" plane by displaying pointing vector arrows pointing in the "+y" direction for a single particle setup.

$$= \frac{\sigma\langle \mathbf{S} \rangle}{C} + \omega\gamma_e\langle \mathbf{L}_e \rangle$$

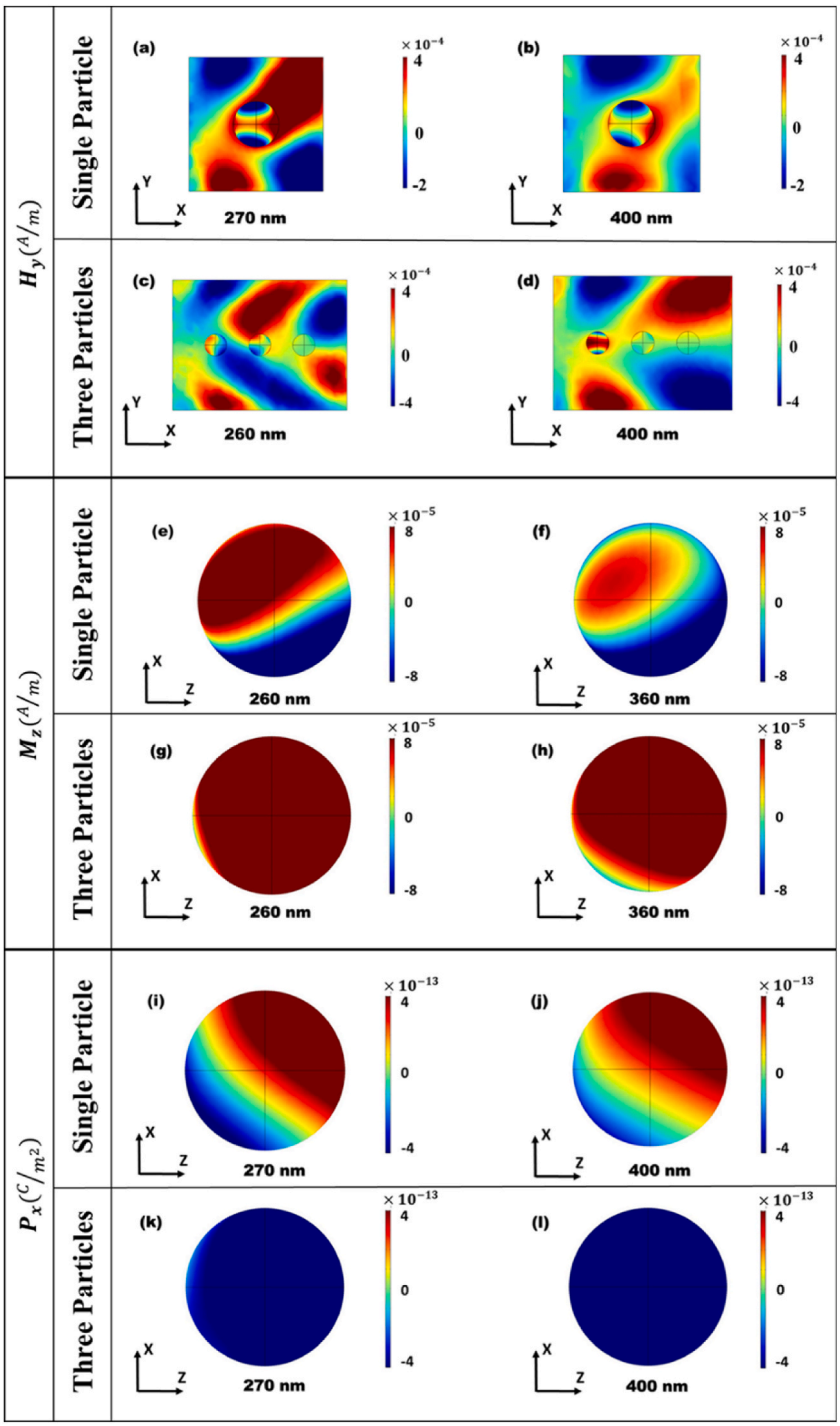


**Fig. 6.** Illustrates magnetic field ($\mathbf{H}_y$) distribution on the gold substrate (note: the incident angle of light is set at 45°). Fig. 6(a and b) provides a graphical representation of the uneven distribution of the scattered field where symmetric scattering occurs, as depicted in Fig. 6(c and d). The magnetization (Fig. 6(e–h)) and polarization (Fig. 6(i–l)) of the chiral particle in presence of other particles behave quite differently in comparison with the independently placed single chiral particle. (For interpretation of the references to colour in this figure legend, the reader is referred to the Web version of this article.)

Here, $\langle \mathbf{S} \rangle = \frac{1}{2}\,\mathrm{Re}[\mathbf{E} \times \mathbf{H}^*]$ is the time average Poynting vector, and $'\sigma'$ is the cross section of the vacuum. The symbol $'\mathbf{E}'$ represents the electric field vector. It describes the strength and direction of the electric field associated with the incident light. The complex conjugate of the magnetic field vector is denoted by the symbol $'\mathbf{H}^*'$, and the cross-product operation is denoted by the sign ( $\times$ ). It is used to figure out the cross product of two vectors. In this instance, it is used to compute the cross product between the electric field vector and the magnetic field vector's complex conjugate.

However, when considering the three particle chiral setups shown in Fig. 2, we did not observe the emergence of any lateral force. In Fig. 5(a) we noticed that there was no effect of the electric field in the non-sorting region of the chiral material (240 nm) for three particles setup. However, in Fig. 5(b and d), we found desired result of an electric field dipole in the sorting region (240 nm and 400 nm) for the single particle setup, whereas Fig. 5(a–c) did not show the same phenomenon.

Here in Fig. 5(b–d), when a plane-polarized light interacts with a single chiral particle; the particle's asymmetric structure induces an electric field dipole within it. The incident light's electric field induces a rotational force on this dipole, which in turn generates spin angular momentum. The spin angular momentum affects the scattering and absorption properties of the particle, leading to modifications in its interaction with light. The interplay between spin angular momentum and the surrounding electromagnetic field results in a lateral force toward the '+y' direction acting on the particle, perpendicular to the light's direction. However, we may contrast the differences between Fig. 5(e and f). The incident light's energy flow direction and intensity are shown by the Poynting vector. The arrows of the Poynting vectors are dispersed in various directions in Fig. 5(e). However, in Fig. 5(f), all the Poynting vector arrows point in the same direction (in the direction of '+Y'). The Poynting vector arrows are oriented in the direction of the chiral lateral force in the area where it occurs. This indicates the direction of energy transfer associated with the incident light.

When a solitary chiral particle is positioned above a substrate, it undergoes a lateral force in the 'y' direction. To visually comprehend this phenomenon, we analyze the magnetic field ($H_y$) patterns of the gold substrate at wavelengths of 270 nm and 400 nm. Fig. 6(a and b) provides a graphical representation of the uneven distribution of the scattered field. These patterns demonstrate that the configuration of a single chiral particle above the substrate yields asymmetric scattering, resulting in the generation of a lateral force. However, when a chiral particle is placed above a substrate along with plasmonic and dielectric particles, the substrate produces symmetric scattering, as depicted in Fig. 6(c and d). This observation highlights that the interaction between a chiral particle and the substrate leads to distinctive scattering behaviors depending on the presence of other types of particles. The asymmetric scattering field generated by the chiral particle-substrate configuration gives rise to the lateral force experienced by the chiral particle alone [27]. Conversely, when combined with plasmonic and dielectric particles, the substrate's scattering behavior becomes symmetrical, and the lateral force becomes absent.

If we give a much deeper look, a very interesting phenomenon arises, which has never been reported before to the best of our knowledge. For example-the presence of other particles suppresses the scattering mechanism of the chiral particle. For example-the magnetic and electric dipole moment are affected significantly in the presence of the other particles. As shown in Fig. 6(e–l), the magnetization and polarization of the chiral particle in the presence of other particles behave quite differently in comparison with the independently placed single chiral particle (near the substrate). Ultimately, due to this suppression, the lateral force on the chiral

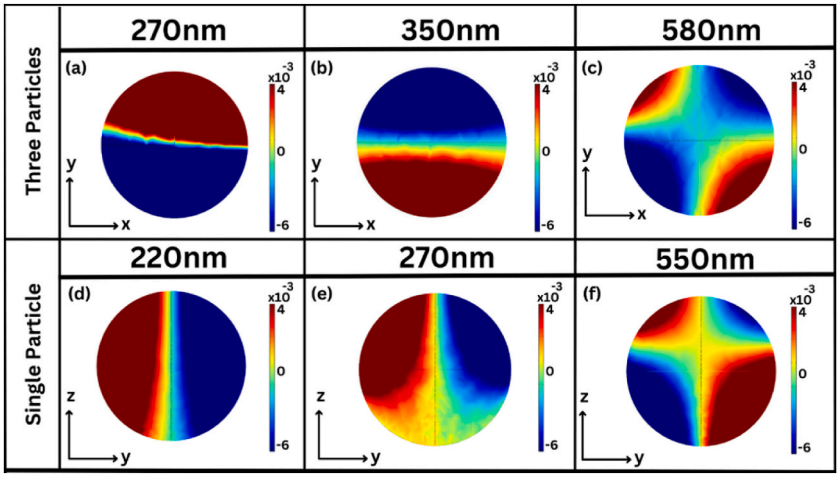


**Fig. 7.** Illustrates the impact of the electric field profile on dielectric particle in different configurations and wavelengths (note: the incident angle of light is set at 45°). (a) In a three-particle configuration with a wavelength of 220 nm, a full wave simulation displays the nonsporting area for the dielectric in the presence of an electric field dipole. Fig. 7(b–e) we can see that similar electric dipole has been induced in the dielectric particle at the wavelengths of 350 nm [multiple particles] and 270 nm [single particle] (where the net time averaged force is negative). (c) It shows that the electric field $\mathbf{E}_x$ generates a quadrupole at 570 nm in a three-particle arrangement, leading to the dielectric pulling force. (d) It demonstrates the electric field dipole effect in a region of 220 nm in the single particle configuration. (f) For the single-particle arrangement, in the area of 550 nm, where the particle forms a quadrupole and produces the dielectric pulling force, these findings shed light on the processes that underlie the optical forces that affect dielectric particle.

particle vanishes as shown in Fig. 2. Impacting the dynamics of the other particle based on another nearby particle is a very recent area of research [50–52]. Though such an impact has been discussed for dielectric particle due to the presence of nearby plasmonic particle (formation of an induced magnetic dipole in the dielectric particle), to the best of our knowledge, such an impact has never been investigated for the chiral particles in presence of other particles in a plasmonic substrate. A further investigation on this issue may be carried on in any of our future works.

In conclusion, the Poynting vector and spin angular momentum both play a role in the production of the chiral lateral force. The electromagnetic field that is rotated by the chiral particle's electric field dipole gives birth to spin angular momentum. The Poynting vector represents the energy flow associated with the incident light's direction and intensity. The chiral particle's scattering and absorption characteristics, as well as the momentum transfer from the incident light, are affected by the interaction between spin angular momentum and the Poynting vector. They work together to produce the chiral lateral force on a single chiral particle placed near (above) the plasmonic substrate.

### 3.2. Sorting of single dielectric particle: origin of the optical pulling force

A setup with a dielectric particle is shown in Fig. 3(c). Here, a light with a 45-degree oblique angle illuminates a dielectric particle, which experienced a pulling force (cf. Fig. 3(d)). The interaction between the incident light and the particle along with the plasmonic structure causes this force, which is opposite to the direction of light propagation. SPP waves produced by the nanostructures propagate and create an interference pattern in the middle.

From Fig. 7(b–e) we can see that electric dipole has been induced in the dielectric particle at the wavelengths of 270 nm [single particle] and 350 nm [multiple particles] (where the net time-averaged force is negative). For this particular wavelength (the regions of dipole formation), we can consider the time-averaged force on the dielectric particle from aforementioned Eq. (4) considering the validity of dipolar approximation as:

$$\langle \mathbf{F}\ \text{Dipole}\ \rangle = \frac{1}{2}[\mathrm{Re}\ [(\nabla \mathbf{E}^{*}) \bullet \mathbf{p}\ ]]$$

Here, the induced dipole moment is represented as, $\mathbf{p} = \alpha_0 \mathbf{E}^{\mathrm{loc}}$, where $\mathbf{E}^{\mathrm{loc}}$ denotes the local electric field. Notably, the local electric field above the substrate comprises two components: the incident field ($\mathbf{E}^{0}(\mathrm{r})$) and the scattering field ($\mathbf{E}^{\mathrm{D}}(\mathrm{r})$). To further enhance our understanding, the introduction of an effective polarizability tensor [24] allows us to express the induced dipole moment as $\mathbf{p} = \widehat{\alpha}\mathbf{E}^{0}$. Furthermore, by applying field superposition, we can break down the optical force acting along the interface into two separate terms:

$$\mathbf{F}_{\mathrm{X}} = \mathbf{F}_{\mathrm{X}}^{\mathrm{O}} + \mathbf{F}_{\mathrm{X}}^{\mathrm{D}} \tag{6}$$

Here

$$\mathbf{F}_{\mathrm{X}}^{\mathrm{O}} = \frac{1}{2}\ \mathrm{k_X}\ \left[\mathrm{Im}\ (\alpha_{\mathrm{XX}})\ \left|\mathbf{E}_{\mathrm{X}}^{\mathrm{O}}\right|^2 + \mathrm{Im}\ (\alpha_{\mathrm{ZZ}})\ \left|\mathbf{E}_{\mathrm{Z}}^{\mathrm{O}}\right|^2\right] \tag{7}$$

This $F_X^O$ cannot be negative [25]. $(\alpha_{XX})$ and $(\alpha_{ZZ})$ are the diagonal element that can be expressed as:

$$\alpha_{\mathrm{XX}} = \frac{\alpha_0}{1 - \alpha_0 \omega^2 \mu_0 \mathrm{G}_{\mathrm{XX}}^{\mathrm{R}}(\mathrm{r}_0, \mathrm{r}_0)}$$

$$\alpha_{\mathrm{ZZ}} = \frac{\alpha_0}{1 - \alpha_0 \omega^2 \mu_0 \mathrm{G}_{\mathrm{zz}}^{\mathrm{R}}(\mathrm{r}_0, \mathrm{r}_0)}$$

On the other hand, when evaluated near the surface plasmon resonance, where Re $(\varepsilon_m + \varepsilon_s \approx 0)$, for a low absorbing surface with $\mathrm{Re}(\varepsilon_s) < 0$ and far from configurational resonance, $\mathbf{F}_{\mathrm{X}}^{\mathrm{D}}$ in Eq (6) can be expressed as:

$$\mathbf{F}_{\mathrm{X}}^{\mathrm{D}} \approx -\frac{\mathrm{k}_{\mathrm{SPP}}^4}{8\varepsilon_0}\ \frac{\mathrm{k}_{\mathrm{SPP}}^3}{\mathrm{k}^3}\ |\alpha_0|^2 \left|\mathbf{E}^{0}\right|^2\ \sin(2\theta)\ \sin[2(\mathrm{k_Z z_0}\ + \varphi)] \times \exp\left(-2\sqrt{\mathrm{k}_{\mathrm{SPP}}^2 - \mathrm{k}^2}\ \mathrm{z}_0\right) \tag{8}$$

Here, ' $z_0$' denotes the height at which the particle is positioned above the substrate, φ is related to the phase of the reflection coefficient, and $\mathbf{E}^0$ represents the local electric field component above the substrate.

One can see from Eq (8) that $\mathbf{F}_{\mathrm{X}}^{\mathrm{D}}$ depends strongly [24] on the SPP wavevector $\mathrm{k_{SPP}}(\propto \mathrm{k}_{\mathrm{SPP}}^7 \exp(-2\sqrt{\mathrm{k}_{\mathrm{SPP}}^2 - \mathrm{k}^2}\, \mathrm{z}_0))$. The force $F_X^D$ can be either positive or negative and this is the component of the total force in Eq (6), which is responsible for the optical pulling force of the dielectric particle placed near (over) a plasmonic surface.

From Fig. 7(a and c) and (d and f), we can see pole fermentation within the dielectric scattered that is placed on our set-up of the gold substrate (for both three-particle and single-particle setups). It is a configuration of electric charges that creates a particular distribution of the electric field. It is a bit surprising observation that the resulting electric field has a quadrupole moment at a wavelength of 580 nm and 550 nm which is a measure of the strength and orientation of the field. The particle should be considered a Rayleigh particle at these wavelength regions. Though, at the Rayleigh regime, the formation of multipole is a bit unusual, such an observation was also reported previously in Ref. [53]. The quadrupole moment is proportional to the product of the charge magnitude "q" and the distance "d" between the charges.

Eq (6) of dipolar force may not be a valid approximation to explain the optical pulling force for the dielectric particle over a substrate at those regions of wavelengths. Though ref [25] demonstrated plasmon polariton assisted optical pulling force for dipolar sized 'dielectric' particle, it was also clearly mentioned in Ref. [25]:

> "The nature of the pulling force in Refs. [21,54] is based on the redistribution of scattering due to interaction of multipoles inside the scattering object. Thus, this force would be absent for particles having only an electric dipole moment, which is the type of particles described in our paper."

The time averaged total force was calculated in Ref. [25] using stress tensor method (by applying full wave analysis) for dielectric particles. We have also done the same. The only difference is the observation of such multipoles. But the results of total time averaged force do not differ. Just we have to provide an explanation in terms of the field-generated multipole moments in order to identify the cause of the optical pulling in a dielectric particle for these wavelength regions. From Eq (4), we can write the time-averaged force for this case considering multipolar response:

$$\langle \mathbf{F} \rangle = \langle \mathbf{F} \text{ Dipole (Generic)} \rangle + \frac{1}{4}\mathrm{Re}[(\nabla\nabla\mathbf{E}^*) \bullet \mathbf{Q}_e] - \frac{k^5}{40\pi\varepsilon_0}\mathrm{Re}[\mathbf{Q}_e \bullet \mathbf{p}^*]$$

Total force can be classified by two terms [23,43,55–57].

$$\mathbf{F} = \mathbf{F}_{\text{incident}} + \mathbf{F}_{\text{interference}} \tag{9}$$

here,

$$\mathbf{F}_{\text{incident}} = \mathbf{F}_p + \mathbf{F}_m + \mathbf{F}_{Qe}$$

and

$$\mathbf{F}_{\text{interference}} = \mathbf{F}_{pm} + \mathbf{F}_{Qep}$$

So, the total force can be calculated,

$$\langle \mathbf{F} \rangle = \mathbf{F}_p + \mathbf{F}_m + \mathbf{F}_{Qe} + \mathbf{F}_{pm} + \mathbf{F}_{Qep} \tag{10}$$

The five terms are the contributions from the electric dipole, magnetic dipole, electric quadrupole, electric–magnetic dipole interference, and electric dipole–quadrupole interference respectively.

The multipolar terms above can be expanded as:

$$F_p = \frac{1}{2}\mathrm{Re}[(\nabla\mathbf{E}^*) \bullet \mathbf{p}];\ \mathbf{F}_m = \frac{1}{2}\mathrm{Re}[(\nabla\mathbf{B}^*) \bullet \mathbf{m}];\ \mathbf{F}_{Qe} = \frac{1}{4}\mathrm{Re}[(\nabla\nabla\mathbf{E}^*) \bullet \mathbf{Q}_e];$$

$$\mathbf{F}_{pm} = -\frac{k^4}{12\pi\varepsilon_0 c}\mathrm{Re}[\mathbf{p} \times \mathbf{m}^*];\ F_{Qep} = -\frac{k^5}{40\pi\varepsilon_0}\mathrm{Re}[\mathbf{Q}_e : \mathbf{p}^*]$$

In the equations above, $\mathbf{E}$ and $\mathbf{H}$ are the incident electric and magnetic field vectors, $\mathbf{p} = \alpha_e\mathbf{E}$, $\mathbf{m} = \alpha_m\mathbf{H}$, $\mathbf{Q}_e = \left(\frac{\gamma_e}{2}\right)(\nabla\mathbf{E} + \nabla\mathbf{E}^T)$ are the induced electric dipole, magnetic and electric quadrupole momentum respectively. Additionally, it is important to note that $\alpha_e, \alpha_m$ and $\gamma_e$ are complex polarizabilities, which can be expanded as follows: $\alpha_e = i6\pi\varepsilon_0\frac{a_1}{k^3}$, $\alpha_m = i6\pi\mu_0\frac{b_1}{k^3}$, and $\gamma_e = i40\pi\varepsilon_0\frac{a_2}{k^5}$, where $a_1$, $b_1$ and $a_2$ are the Mie coefficients and $'\mathbf{k}'$ is the wave vector.

Now, we can express Eq. (10) more explicitly as:

$$\langle \mathbf{F} \rangle = \frac{1}{2}\mathrm{Re}[(\nabla\mathbf{E}^*) \bullet \mathbf{p}] + \frac{1}{2}\mathrm{Re}[(\nabla\mathbf{B}^*) \bullet \mathbf{m}] + \frac{1}{4}\mathrm{Re}[(\nabla\nabla\mathbf{E}^*) \bullet \mathbf{Q}_e] - \frac{k^4}{12\pi\varepsilon_0 c}\mathrm{Re}[\mathbf{p} \times \mathbf{m}^*] - \frac{k^5}{40\pi\varepsilon_0}\mathrm{Re}[\mathbf{Q}_e : \mathbf{p}^*] \tag{11}$$

According to Eq. (11), it is evident that the components in $\mathbf{F}_{\text{interference}}$ are responsible for the development of the optical pulling force. On the other hand, the components in $\mathbf{F}_{\text{incident}}$ are responsible for the generation of optical pushing force [23,43].

From Fig. 7(c) [three particle setups] and 7(f) [single particle setup], we can observe the apparent pole formation within a dielectric scatterer at wavelengths of 580 nm and 550 nm, respectively. Analyzing the electric field profiles, we can witness the occurrence of interference between electric dipoles and quadrupoles within the mentioned object, triggered by the optical pulling force experienced by the dielectric particle. According to Eq. (11), the presence of electric dipole-quadrupole interference leads to a momentum contribution that is primarily responsible for the emergence of an optical pulling force in a dielectric object for these regions of wavelengths.

Furthermore, looking at Fig. 7(a) and (d), electric dipole moments observed the same dielectric particle at wavelength 220 nm. Dielectric particles exhibit an optical pushing force at this wavelength. According to Eq. (9), the momentum contribution from the electric dipole typically leads toward the exertion of an optical pushing force. Hence, we can conclude that, the interaction between electric dipoles and quadrupoles, known as electric dipole-quadrupole interference, is responsible for the optical pulling force.

This interaction causes the $\mathbf{F}_{\text{interference}}$ portion of Eq. (9) to become greater than the $\mathbf{F}_{\text{incident}}$ portion, resulting in the dielectric object being pulled towards the "-x" direction. Conversely, the excitation of electric dipoles leads to the $\mathbf{F}_{\text{incident}}$ component of Eq. (9) being greater than the $\mathbf{F}_{\text{interference}}$ part. As a result, the object is pushed towards the "+x" direction, experiencing an optical pushing force.

### 3.3. Sorting of single plasmonic particle: origin of the optical pushing force

A setup with a plasmonic particle (gold) is shown in Fig. 3(e). Here, a light with a 45-degree oblique angle illuminates a plasmonic particle, which experienced a pushing force in the sorting regions of wavelengths. The interaction between the incident light and the particle along with the plasmonic structure causes this force, which is in the same direction of light propagation. SPP waves produced by the nanostructures propagate and create an interference pattern in the middle.

In both cases (three particle and single particle setups), the plasmonic particle experiences an optical pushing force at wavelengths of 250 nm–550 nm. It is important to note that ref [25] only demonstrated plasmon polariton assisted optical pulling force for dipolar sized 'dielectric' particle. Later, we investigated the plasmon polariton assisted pulling force for Mie sized 'dielectric' particle in Ref. [40]. However, we shined light from the bottom of the metasurface in Ref. [40].

Then a question arises: Why doesn't the pulling force arise when the plasmonic particle is positioned above the flat plasmonic substrate, despite the continued presence of the propagating Surface Plasmon Polariton (SPP) and nearly identical external conditions (Note: the internal condition is different due to inherent absorption of the plasmonic particle)?

The answer to the aforementioned question lies on the property of the plasmonic particles. The absorption of the plasmonic particle is playing the most vital role here. Though the equations presented in (6)-(8) are valid equations strictly for both absorbing and non-absorbing particles, the pulling force term in Eq (6) remains valid when: Multipoles are not created within the object. We observe in Fig. 8(a–f) that multipoles have been created in plasmonic particle for both the cases (independently placed single plasmonic particle and also for the case when other particles are present). As a result, Eq (6) may not remain a valid equation to describe the dynamics of the plasmonic particle. Ref [25] only demonstrated plasmon polariton assisted optical pulling force for dipolar sized 'dielectric' particle. It was also clearly mentioned in Ref. [25]:

> "The nature of the pulling force in Refs. [19,21] is based on the redistribution of scattering due to interaction of multipoles inside the scattering object. Thus, this force would be absent for particles having only an electric dipole moment, which is the type of particles described in our paper."

The impact of absorption (low to high) is also not well understood for Eq (6). According to Fig. 3(f), the single plasmonic particle (or the plasmonic particle in the cluster (Fig. 2)) does not experience pulling force for the sorting regions of wavelengths. But the pulling force arises in the non-sorting region. We observed such a situation (both pushing & pulling) previously for another set-up: particle (Mie sized) placed in half air-water interface [58]. However, according to our previous and current observations, the impact of internal absorption of a particle most of the times leads to pushing force whether the set-up: particle placed over a plasmonic substrate or particle placed in the half air-water interface.

Is there any way to predict the pushing and pulling force for an absorbing particle such as a plasmonic particle?

Such a way may better be explained based on Lorentz force distribution equations [38,51] instead of strict dipolar approximation-based equations given in Eqs. (6)–(8) [in fact the electric field profiles in Fig. 8 (a)–(f) suggest that dipolar approximation does not remain valid due to the creation of multipoles]. To gain a deeper understanding of the pushing phenomenon, we need to discuss the force contribution from the bound current and charge induced within the active plasmonic nanoparticle. In the case where plasmonic particle experience an optical pushing force ('+x'-direction), the current density profile remains the same for both three-particle and single-particle configurations. This similarity is demonstrated in Fig. 9(a and b) and 9(d, e). Conversely, when examining Fig. 9(c) and (f) in the region where plasmonic particles are subjected to a pulling force ('-x'-direction), the current density profile exhibits a complete reversal compared to the pushing region ('+x'-direction). Previously the reversal of current density inside

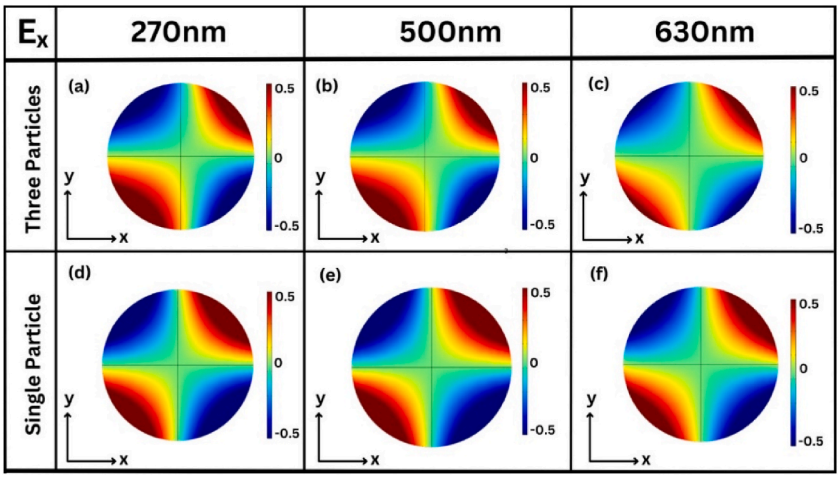


**Fig. 8.** Illustrates the impact of the electric field profile on plasmonic particle in different configurations and wavelengths (note: the incident angle of light is set at 45°). Fig. 8(a–f) shows that multipoles have been created in plasmonic particle for both cases (independently placed single plasmonic particle and also for the case when other particles are present).

the plasmonic particle was observed [40,59,60] when the particle experiences an optical pulling force. This fact will be explained next based on the Lorentz force dynamics.

The emergence of optical pushing forces in the plasmonic nanospheres can be explained by the momentum contribution of free carriers within them. Here, two separate forces combine to create a net total force that is the sum of their individual effects. It can be explained by the Lorentz force distribution [40,61], where Eq. (2) can be written according to Minkowski's theorem:

$$\oint \langle \overline{\overline{\mathbf{T}}}^{\text{out}} \rangle . \text{ds} = \langle \mathbf{F}_{\text{total}} \rangle = \langle \mathbf{F}_{\text{Surface Mink}} \rangle + \langle \mathbf{F}_{\text{Bulk Mink}} \rangle \tag{12}$$

Here,

$$\langle \mathbf{F}_{\text{Mink.}}^{\text{Bulk}} \rangle = \frac{1}{2} \text{Re} \left[ \int \left[ \rho_{\text{free}} \mathbf{E}_{\text{in}} + \mathbf{J}_{\text{free}}(\text{in}) \times \mu_0 \mathbf{H}_{\text{in}} \right] \text{dv} \right] \tag{13}$$

$$\langle \mathbf{F}_{\text{Mink.}}^{\text{Surface}} \rangle = \frac{1}{2} \text{Re} \left[ \oint \left[ -\frac{1}{2} |\mathbf{E}_{\text{Surf}}|^2 \nabla \varepsilon \right] \text{ds} \right] \tag{14}$$

here, "surf" and "in" denotes the surface of the scatterer and the interior of the scatter, respectively.

Now, Eq. (12) can be written as,

$$\langle \mathbf{F}_{\text{total}} \rangle = \text{Re} \left[ \oint \left[ -\frac{1}{2} |\mathbf{E}_{\text{Surf}}|^2 \nabla \varepsilon \right] \text{ds} \right] + \frac{1}{2} \text{Re} \left[ \int \left[ \rho_{\text{free}} \, \mathbf{E}_{\text{in}} + \mathbf{J}_{\text{free}} \, (\text{in}) \times \mu_0 \mathbf{H}_{\text{in}} \right] \right] \text{dv} \tag{15}$$

in the case of lossless dielectric objects, the bulk force of Minkowski term, as indicated by Eq. (13), usually zero because there are no free charge densities ($\rho_{\text{free}}$) or free current densities ($\boldsymbol{J}_{\text{free}}(\boldsymbol{in})$) present within the object. So, for a lossless object (such as a non-absorbing dielectric object), total net force comes from the first term (surface force) of Eq. (12), and it's called Helmholtz force. In the context of a lossy object, such as the plasmonic object in our scenario, the overall force is influenced by both terms described in Eq. (12), and the bulk force is always non-zero. For a plasmonic or absorbing particle's total time averaged force is usually determined by both surface force and bulk force component. In the case of lossy objects, the bulk force described in Eq. (13), which strongly relies on the presence of free current density, typically leads to a positive bulk force [62]. Although this has been known earlier, recent reports in the literature [40,61,63] have discovered that manipulating both terms in Eq. (12) allows for the achievement of an overall pulling force on a lossy object. Usually, this reversal of force occurs at the point where the reversal of current density of the plasmonic scatterer takes place [55].

On closer inspection, it becomes clear that the three-particle configuration in Fig. 9(a and b) does not experience a current density reversal. Additionally, the sorting zone in Fig. 9(d and e) similarly exhibits no current density reversal at 270 nm and 500 nm. However, a current density reversal in Fig. 9(f) at 630 nm shows the presence of a pulling force within that specific range. It is important to note that the lack of current density reversal causes a pushing force for the plasmonic particle between the wavelengths of 250 nm and 550 nm.

## 4. Conclusion

In conclusion, our optical configuration presents a method for particle sorting through the utilization of a plasmonic substrate illuminated by a linearly polarized light beam. This interaction induces the generation of surface plasmon polaritons (SPPs) on the substrate's surface, leading to the formation of interference scatter waves. The resultant complex plasmonic field gives rise to various effects, such as a dipole electric field, a Poynting vector acting on chiral entities, dominant electric quadrupoles in Rayleigh-sized dielectric scatters, and a reversal of current density in the plasmonic nanoparticle in the non-sorting region. Consequently, these phenomena produce distinct forces on different types of particles, especially independently placed single chiral or dielectric or plasmonic particle. In the sorting regions of wavelengths, the chiral particle experiences an optical lateral force, the dielectric particle is subject to optical pulling, while the plasmonic particle undergoes an optical pushing force. Therefore, a sorting domain can be showcased as the particles experience different forces in different directions. However, the proposed technique does not work for the multi-particle set-up. The physical reasons for all the aforementioned observations have been explained both analytically and qualitatively. Optical sorting for future industrial applications can be utilized instead of using several costly chemicals. Overall, the efficient and precise sorting of particles using the proposed setup could help in the development of new technologies and products, improving the quality and efficiency of existing processes.

## Data availability

Data underlying the results presented in this paper are not publicly available at this time but may be obtained from the authors upon reasonable request.

## CRediT authorship contribution statement

**Jannatul Shahrin Shoshi:** Writing – original draft, Validation, Software, Methodology, Formal analysis, Data curation,

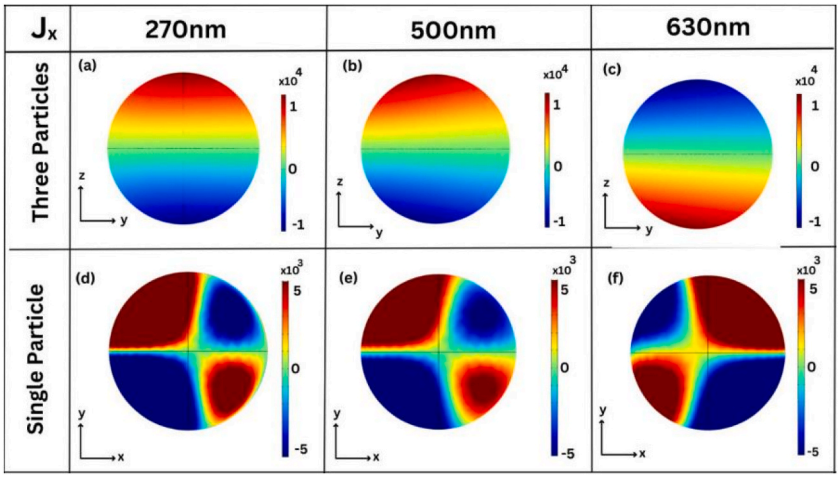


**Fig. 9.** No current density reversal of plasmonic particles is observed over our three particle and single particle setups at incident beam wavelengths of 270 nm and 500 nm, as shown in Fig. 9(a, b) and (d, e). Fig. 9(c) and (f) represent that at 630 nm, where plasmonic particles are subjected to a pulling force ('-x'-direction), the current density profile exhibits a complete reversal compared to the pushing region ('+x'-direction), (note: the incident angle of light is set at 45°).

Conceptualization. **M.R.C Mahdy:** Writing – review & editing, Writing – original draft, Visualization, Supervision, Resources, Project administration, Investigation, Funding acquisition. **Mostafizur Rahman Rana:** Writing – original draft, Visualization, Software, Methodology, Formal analysis, Data curation, Conceptualization.

## Declaration of competing interest

The authors declare that they have no known competing financial interests or personal relationships that could have appeared to influence the work reported in this paper.

## Acknowledgments

M.R.C. Mahdy acknowledges the support of North South University's (NSU) internal CTRGC grant 2022-23 (Approved by the members of BOT, NSU, Bangladesh).

## Appendix A. Supplementary data

Supplementary data to this article can be found online at https://doi.org/10.1016/j.heliyon.2024.e26722.

## References

[1] M. Hoeb, J.O. Rädler, S. Klein, M. Stutzmann, M.S. Brandt, Light-induced Dielectrophoretic manipulation of DNA, Biophys. J. 93 (2007) 1032–1038, https://doi.org/10.1529/biophysj.106.101188.
[2] A. Ashkin, J.M. Dziedzic, Optical trapping and manipulation of viruses and bacteria, Science 235 (1987) 1517–1520, https://doi.org/10.1126/science.3547653, 80-.
[3] F.M. Fazal, S.M. Block, Optical tweezers study life under tension, Nat. Photonics 5 (2011) 318–321.
[4] V. Demergis, E.L. Florin, Ultrastrong optical binding of metallic nanoparticles, Nano Lett. 12 (2012) 5756–5760, https://doi.org/10.1021/nl303035p.
[5] D. Gao, W. Ding, M. Nieto-Vesperinas, X. Ding, M. Rahman, T. Zhang, C. Lim, C.-W. Qiu, Optical manipulation from the microscale to the nanoscale: fundamentals, advances and prospects, Light Sci. Appl. 6 (2017) e17039–e17039, https://doi.org/10.1038/lsa.2017.39.
[6] A. Ashkin, Atomic-beam Deflection by resonance-radiation pressure, Phys. Rev. Lett. 25 (1970) 1321–1324, https://doi.org/10.1103/PhysRevLett.25.1321.
[7] R. Zhu, T. Avsievich, A. Popov, I. Meglinski, Optical tweezers in studies of red Blood cells, Cells 9 (2020) 1–27, https://doi.org/10.3390/cells9030545.
[8] H. Tan, H. Hu, L. Huang, K. Qian, Plasmonic tweezers for optical manipulation and biomedical applications, Analyst 145 (2020) 5699–5712, https://doi.org/10.1039/d0an00577k.
[9] M. Dienerowitz, M. Mazilu, K. Dholakia, Optical manipulation of nanoparticles: a review, SPIE Rev 1 (2010) 1–32, https://doi.org/10.1117/1.2992045.
[10] A.H.J. Yang, S.D. Moore, B.S. Schmidt, M. Klug, M. Lipson, D. Erickson, Optical manipulation of nanoparticles and biomolecules in sub-wavelength slot waveguides, Nature 457 (2009) 71–75, https://doi.org/10.1038/nature07593.
[11] M. Zhang, X. Gong, W. Wen, Manipulation of microfluidic droplets by electrorheological fluid, Electrophoresis 30 (2009) 3116–3123, https://doi.org/10.1002/elps.200900119.
[12] K.C. Neuman, A. Nagy, Single-molecule force spectroscopy: optical tweezers, magnetic tweezers and atomic force microscopy, Nat. Methods 5 (2008) 491–505, https://doi.org/10.1038/nmeth.1218.
[13] P. V Cornish, T. Ha, A survey of single-molecule techniques in chemical biology, ACS Chem. Biol. 2 (2007) 53–61.
[14] J. Ye, H.J. Kimble, H. Katori, Quantum state engineering and precision metrology using state-insensitive light traps, Science 320 (2008) 1734–1738, 80-.

[15] S. Stellmer, B. Pasquiou, R. Grimm, F. Schreck, Laser Cooling to quantum degeneracy, Phys. Rev. Lett. 110 (2013) 263003, https://doi.org/10.1103/PhysRevLett.110.263003.
[16] M. Mansuripur, Radiation pressure and the linear momentum of the electromagnetic field, Opt Express 12 (2004) 5375–5401.
[17] C.-W. Qiu, W. Ding, M.R.C. Mahdy, D. Gao, T. Zhang, F.C. Cheong, A. Dogariu, Z. Wang, C.T. Lim, Photon momentum transfer in inhomogeneous dielectric mixtures and induced tractor beams, Light Sci. Appl. 4 (2015) e278, e278.
[18] M. Bethune-Waddell, K.J. Chau, Simulations of radiation pressure experiments narrow down the energy and momentum of light in matter, Rep. Prog. Phys. 78 (2015) 122401.
[19] C. Baxter, R. Loudon, Radiation pressure and the photon momentum in dielectrics, J. Mod. Opt. 57 (2010) 830–842.
[20] O. Brzobohatý, V. Karásek, M. Šiler, L. Chvátal, T. Čižmár, P. Zemánek, Experimental demonstration of optical transport, sorting and self-arrangement using a 'tractor beam, Nat. Photonics 7 (2013) 123–127.
[21] V. Kajorndejnukul, W. Ding, S. Sukhov, C.W. Qiu, A. Dogariu, Linear momentum increase and negative optical forces at dielectric interface, Nat. Photonics 7 (2013) 787–790, https://doi.org/10.1038/nphoton.2013.192.
[22] A. Novitsky, C.W. Qiu, H. Wang, Single gradientless light beam drags particles as tractor beams, Phys. Rev. Lett. 107 (2011) 1–4, https://doi.org/10.1103/PhysRevLett.107.203601.
[23] J. Chen, J. Ng, Z. Lin, C.T. Chan, Optical pulling force, Nat. Photonics 5 (2011) 531–534.
[24] M.I. Petrov, S.V. Sukhov, A.A. Bogdanov, A.S. Shalin, A. Dogariu, Surface plasmon polariton assisted optical pulling force, Laser Photonics Rev 10 (2016) 116–122, https://doi.org/10.1002/lpor.201500173.
[25] T. Zhu, A. Novitsky, Y. Cao, M.R.C. Mahdy, L. Wang, F. Sun, Z. Jiang, W. Ding, Mode conversion enables optical pulling force in photonic crystal waveguides, Appl. Phys. Lett. 111 (2017) 1–7, https://doi.org/10.1063/1.4997924.
[26] T. Zhang, M.R.C. Mahdy, Y. Liu, J.H. Teng, C.T. Lim, Z. Wang, C.-W. Qiu, All-optical chirality-sensitive sorting via reversible lateral forces in interference fields, ACS Nano 11 (2017) 4292–4300.
[27] S.B. Wang, C.T. Chan, Lateral optical force on chiral particles near a surface, Nat. Commun. 5 (2014) 1–8, https://doi.org/10.1038/ncomms4307.
[28] F.J. Rodríguez-Fortuñ, N. Engheta, A. Martínez, A.V. Zayats, Lateral forces on circularly polarizable particles near a surface, Nat. Commun. 6 (2015), https://doi.org/10.1038/ncomms9799.
[29] Y. Shi, T. Zhu, T. Zhang, A. Mazzulla, D.P. Tsai, W. Ding, A.Q. Liu, G. Cipparrone, J.J. Sáenz, C.W. Qiu, Chirality-assisted lateral momentum transfer for bidirectional enantioselective separation, Light Sci. Appl. 9 (2020), https://doi.org/10.1038/s41377-020-0293-0.
[30] A.M. Stalcup, Chiral separations, Annu. Rev. Anal. Chem. 3 (2010) 341–363.
[31] Z. Wang, H. Wang, S. Lin, S. Ahmed, S. Angers, E.H. Sargent, S.O. Kelley, Nanoparticle amplification labeling for high-performance magnetic cell sorting, Nano Lett. 22 (2022) 4774–4783.
[32] F. Bonaccorso, M. Zerbetto, A.C. Ferrari, V. Amendola, Sorting nanoparticles by centrifugal fields in clean media, J. Phys. Chem. C 117 (2013) 13217–13229, https://doi.org/10.1021/jp400599g.
[33] K.E. Fong, L.-Y.L. Yung, Localized surface plasmon resonance: a unique property of plasmonic nanoparticles for nucleic acid detection, Nanoscale 5 (2013) 12043, https://doi.org/10.1039/c3nr02257a.
[34] J. Masura, J. Baker, G. Foster, C. Arthur, Laboratory methods for the analysis of microplastics in the marine environment, NOAA Mar. Debris Progr. Natl. (2015) 1–39.
[35] X. Wang, S. Liu, Y. Sun, X. Yu, S.M. Lee, Q. Cheng, T. Wei, J. Gong, J. Robinson, D. Zhang, Preparation of selective organ-targeting (SORT) lipid nanoparticles (LNPs) using multiple technical methods for tissue-specific mRNA delivery, Nat. Protoc. 18 (2023) 265–291.
[36] E. Almaas, I. Brevik, Possible sorting mechanism for microparticles in an evanescent field, Phys. Rev. A 87 (2013) 63826.
[37] M. Ploschner, T. Cizmar, M. Mazilu, A. Di Falco, K. Dholakia, Bidirectional optical sorting of gold nanoparticles, Nano Lett. 12 (2012) 1923–1927.
[38] D.A. Shilkin, E. V Lyubin, M.R. Shcherbakov, M. Lapine, A.A. Fedyanin, Directional optical sorting of silicon nanoparticles, ACS Photonics 4 (2017) 2312–2319.
[39] S.C. Das, M.R.C. Mahdy, M.S. Islam, R. Jani, M.S. Bhuiyan, An optical cluster: near-field optical sorting and separation of plasmonic, dielectric, and chiral nanoparticle, Ann. Phys. 533 (2021) 1–11, https://doi.org/10.1002/andp.202100299.
[40] K. Safkat, M. Rahim, M.R.C. Mahdy, Optical sorting of a plasmonic or dielectric or chiral Mie object using a single metasurface, Ann. Phys. 534 (2022) 2100402, https://doi.org/10.1002/andp.202100402.
[41] M.M. Rahman, A. Al Sayem, M.R.C. Mahdy, M.E. Haque, R. Islam, S.T. Chowdhury, M.A. Matin, Tractor beam for fully immersed multiple objects: long distance pulling, trapping, and rotation with a single optical set-up, Ann. Phys. 527 (2015) 777–793, https://doi.org/10.1002/andp.201500266.
[42] E. Lee, T. Luo, T. Luo, T. Luo, Long-distance optical pulling of nanoparticle in a low index cavity using a single plane wave, Sci. Adv. 6 (2020) 1–9, https://doi.org/10.1126/sciadv.aaz3646.
[43] M.R. Rana, M. Rahim, S.P. Sultana, F.R. Efa, M.R.C. Mahdy, Optical tractor beam for a cluster of plasmonic and dielectric and chiral Mie objects, Opt Commun. 528 (2023) 129040, https://doi.org/10.1016/j.optcom.2022.129040.
[44] N.B. Ahsan, R. Shamim, M.R.C. Mahdy, S.C. Das, H.M. Rivy, C.I. Dolon, M. Hossain, K.M. Faisal, Chiral and plasmonic hybrid dimer pair: reversal of both near- and far-field optical binding forces, JOSA B 37 (2020) 1273–1282.
[45] M.R.C. Mahdy, T. Zhang, S.C. Das, H.M. Rivy, On chip optical tractor beam by surface plasmon polariton, Opt Commun. 463 (2020) 125395, https://doi.org/10.1016/j.optcom.2020.125395.
[46] F. Islam, E.U. Biswas, M.R. Rana, M.R.C. Mahdy, Sierpinski-fractal inspired ultra-broadband UV-NIR meta absorber: Notable impact on the self-stabilization of light-sail or solar-sail, Opt. Mater. 148 (2024) 114838, https://doi.org/10.1016/j.optmat.2024.114838.
[47] P.B. Johnson, R.W. Christy, Optical constants of the noble metals, Phys. Rev. B 6 (1972) 4370–4379, https://doi.org/10.1103/PhysRevB.6.4370.
[48] C.F. Bohren, D.R. Huffman, Absorption and Scattering of Light by Small Particles, John Wiley & Sons, 2008.
[49] I. Lindell, A. Sihvola, S. Tretyakov, A.J. Viitanen, Electromagnetic Waves in Chiral and Bi-isotropic Media, Artech House, 1994.
[50] G. Guo, T. Feng, Y. Xu, Tunable optical pulling force mediated by resonant electromagnetic coupling, Opt. Lett. 43 (2018) 4961, https://doi.org/10.1364/OL.43.004961.
[51] A. Kiselev, O.J.F. Martin, Controlling the magnetic and electric responses of dielectric nanoparticles via near-field coupling, Phys. Rev. B 106 (2022) 205413.
[52] T. Feng, S. Yang, N. Lai, W. Chen, D. Pan, W. Zhang, A.A. Potapov, Z. Liang, Y. Xu, Manipulating light scattering by nanoparticles with magnetoelectric coupling, Phys. Rev. B 102 (2020) 205428.
[53] V.D. Miljković, T. Pakizeh, B. Sepulveda, P. Johansson, M. Käll, Optical forces in plasmonic nanoparticle dimers, J. Phys. Chem. C 114 (2010) 7472–7479, https://doi.org/10.1021/jp911371r.
[54] C. Baxter, R. Loudon, V. Kajorndejnukul, W. Ding, S. Sukhov, C.W. Qiu, A. Dogariu, No Title, (n.d.). https://doi.org/10.1038/nphoton.2013.192..
[55] J. Arlt, K. Dholakia, Generation of high-order Bessel beams by use of an axicon, Opt Commun. 177 (2000) 297–301.
[56] B.A. Kemp, T.M. Grzegorczyk, J.A. Kong, Optical momentum transfer to absorbing Mie particles, Phys. Rev. Lett. 97 (2006) 133902, https://doi.org/10.1103/PhysRevLett.97.133902.
[57] D. McGloin, K. Dholakia, Bessel beams: diffraction in a new light, Contemp. Phys. 46 (2005) 15–28.
[58] M.R.C. Mahdy, H.M. Rivy, Z.R. Jony, N.B. Alam, N. Masud, G.D. Al Quaderi, I.M. Moosa, C.M. Rahman, M. Sohel Rahman, Dielectric or plasmonic Mie object at air–liquid interface: the transferred and the traveling momenta of photon, Chinese Phys. B 29 (2020) 014211, https://doi.org/10.1088/1674-1056/ab5efa.
[59] J. Arlt, K. Dholakia, Generation of high-order Bessel beams by use of an axicon, Opt Commun. 177 (2000) 297–301, https://doi.org/10.1016/S0030-4018(00)00572-1.
[60] M.S. Zia, M.M. Islam, M. Rahim, T. Bhowmick, M.M. Rahman, M.R.C. Mahdy, Dielectric and plasmonic hybrid dimer pair: broadband reversal of optical binding force, Prog. Electromagn. Res. Lett. 101 (2021) 99–105.

[61] C. Jones, B.A. Kemp, C.J. Sheppard, Enhanced radiation pressure reversal on free carriers in nanoparticles and polarization dependence in the Rayleigh regime, Opt. Eng. 60 (2021) 27104, https://doi.org/10.1117/1.OE.60.2.027104.
[62] B.A. Kemp, J.A. Kong, T.M. Grzegorczyk, Reversal of wave momentum in isotropic left-handed media, Phys. Rev. A 75 (2007) 53810.
[63] M.H. Rahaman, B.A. Kemp, Negative force on free carriers in positive index nanoparticles, APL Photonics 2 (2017) 101301, https://doi.org/10.1063/1.4991567.